ACS APPLIED MATERIALS & INTERFACES

Research Article

www.acsami.org

Synthesis of Cobalt Phosphides and Their Application as Anodes for Lithium Ion Batteries

Dan Yang,[†,‡] Jixin Zhu,[†,‡] Xianhong Rui,[†,⊥] Huiteng Tan,[†] Ren Cai,[⊥] Harry E. Hoster,[‡] Denis Y. W. Yu,[‡,§] Huey Hoon Hng,[†] and Qingyu Yan*[,†,‡,§]

[†]School of Materials Science and Engineering, Nanyang Technological University, Singapore 639798, Singapore

[‡]TUM CREATE Research Centre@NTU, Nanyang Technological University, Singapore 637459, Singapore

[§]Energy Research Institute@NTU, Nanyang Technological University, Singapore 637553, Singapore

[⊥]School of Civil and Environmental Engineering, Nanyang Technological University, Singapore 639798, Singapore

Supporting Information

ABSTRACT: A facile thermal decomposing method has been developed for the fabrication of Co_xP nanostructures with controlled size, phase, and shape (e.g., Co_2P rod and spheres, CoP hollow and solid particles). An amorphous carbon layer could be introduced by the carbonization of organic surfactants from the precursors. The electrochemical performance of typical CoP and Co_2P samples as anode materials has been investigated and the CoP hollow nanoparticle with carbon coating layer depicts good capacity retention and high rate capability (e.g., specific capacity of 630 mA h g^{-1} at 0.2 *C* after 100 cycles, and a reversible capacity of 256 mA h g^{-1} can be achieved at a high current rate of 5 *C*).

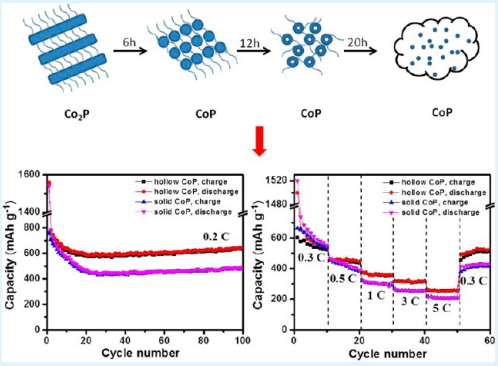

KEYWORDS: *hollow nanoparticles, nanorods, Li storage, cobalt phosphides, oil phase synthesis*

INTRODUCTION

Transition metal phosphides (MP_x, where M = Fe, Co, Ni, etc.) are considered to be alternative anode materials for lithium ion battery (LIB) because of their high gravimetric and volumetric capacities (500−1800 mAh g^{-1}).[1] However, one major drawback that limits their practical application is the drastic volume change generated during the Li^+ intercalation/deintercalation process.[1−3] This volume change can cause pulverization of the initial crystal structure and loss of electrical contact between active materials and the current collector, which lead to poor capacity retention and short cycle life. Constructing materials into nanostructures with controlled morphologies (e.g., nanotubes,[4] nanorods,[5] and hollow spheres[6]) is one attractive approach to address this problem. Such architectures can provide higher interfacial contact area as well as better accommodation for the volume expansion and are expected to lead to a better capability.[7−10] Another challenge for practical application of MP_x is their intrinsically low electronic conductivity. Generally, hybridizing the electrode materials with carbonaceous materials, e.g. carbon shell/network, can effectively enhance the kinetics of charge transfer and improve their lithium storage performance.[11,12] Moreover, the carbon layer can either buffer the strain caused by structural or volume changes, or prevent the agglomeration of active materials during cycling process.[13,14]

Cobalt phosphides (e.g., orthorhombic Co_2P and CoP phases) are expected to be promising anode materials for their relatively low charge−discharge potential,[15] metallic character and good thermal stability.[16] With the advances in recent nanotechnology,[17−19] various synthetic methods have been developed for the synthesis of Co_2P and CoP nanomaterials.[20−32] However, attractive lithium storage properties (e.g., stable cyclability and high rate capability) have not been achieved for Co_2P/CoP anodes owing to the aforementioned issues yet. Herein, we report a solution-phase synthesis of different structured Co_2P and CoP (e.g., particles, rods, hollow spheres, and solid spheres) by decomposing Co-TOP complex in a hot oleylamine (OAm) solution. The effects of synthesis parameters (e.g., injection rate of the precursors and reaction time) on the morphology and phase of the product are investigated in detail. Comparison of the Li storage properties for different nanostructures and phases has been systematically carried out. As shown in the results, control over the shape or microstructure of cobalt phosphides can lead to enhanced Li storage properties. Specifically, the CoP hollow nanoparticles delivered a discharge capacity of 630 mA h g^{-1} during the 100th cycle at a charge/discharge rate of 0.2 *C*. Even at a high rate of

Received: November 28, 2012
Accepted: January 12, 2013
Published: January 12, 2013

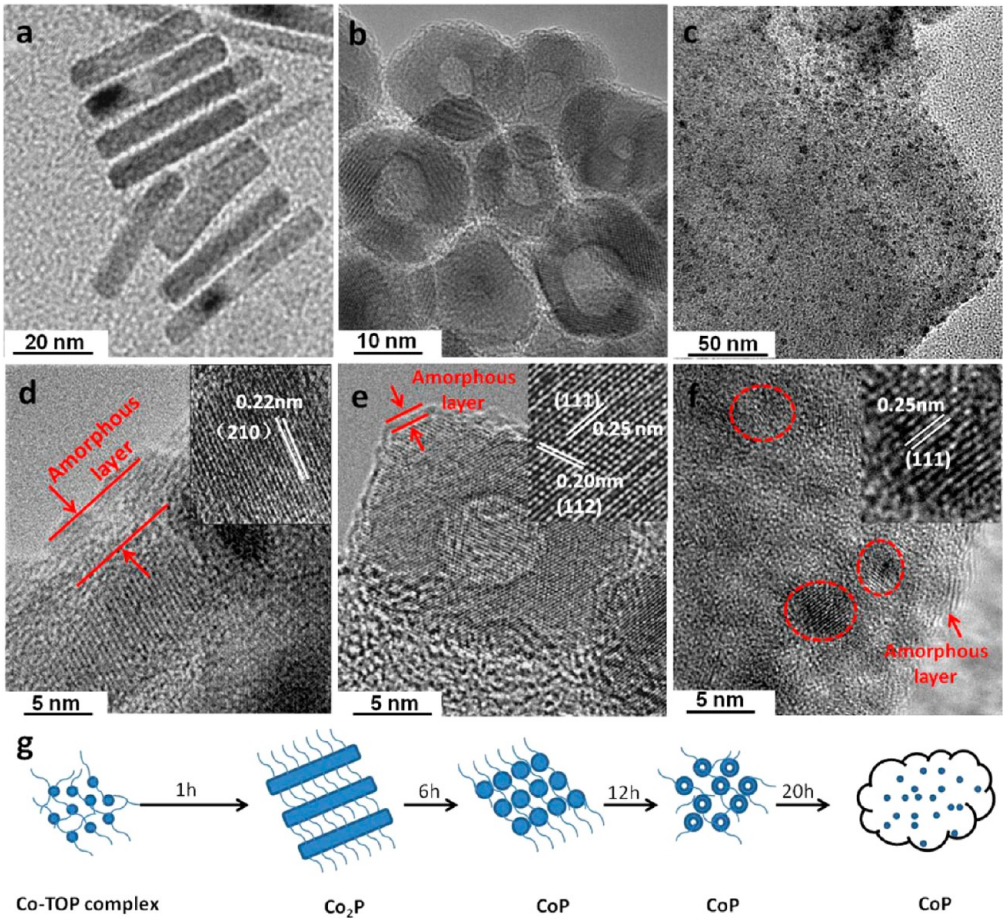

Figure 1. TEM image obtained from different reaction time. (a) Co_2P rods (1 h); (b) CoP hollow spheres (12 h); (c) fine CoP nanoparticles (20 h); (d–f and insets) corresponding HRTEM images of the above Co_xP; (g) scheme of the phase and morphology evolution with duration time.

5 C, a reversible discharge capacity of 256 mA h g^{-1} can be achieved.

EXPERIMENTAL SECTION

Synthesis. All reactions were carried out under an argon (Ar) atmosphere using standard Schlenk line techniques. In a typical synthesis of Co_2P nanorods, 10 mL oleylamine was heated to 100 °C in a Schlenk flask with a reflux condenser by heating mantle. The oleylamine solvent was degassed at 100 °C for 30 min by an oil pump and then heated to 320 °C with a flowing Ar gas during all the process. In the meantime, 0.25 g of Co $(acac)_2$ and 5 mL of TOP were mixed and heated to above 70 °C to yield a light violet Co-TOP complex solution. This Co-TOP complex solution was then injected into the above hot oleylamine solvent dropwisely, yielding a black solution and this system was aged under 320 °C for 1 h. The samples were first washed by ethanol and then washed by the mixture of 3 mL of hexane and 50 mL of ethanol for 3 times. Finally, the samples were dried under vacuum and collected for characterization.

Characterization Techniques. The morphologies of the samples were characterized by a field emission scanning electron microscope (FESEM, JEOLJSM-7600F). The structures of the samples were investigated using a transmission electron microscope (TEM, JEOL 2010) operating at 200 kV. Crystal phases of the samples were identified using X-ray diffractometer (Shimadzu) with Cu KR irradiation. Raman spectra were obtained with a WITec CRM200 confocal Raman microscopy system with a laser wavelength of 488 nm and a spot size of 0.5 mm. To calibrate the wavenumber, the Si peak at 520 cm^{-1} was used as a reference.

Electrochemical Characterization. The as-synthesized samples were annealed in a tube furnace at 450 °C for 2 h under Ar atmosphere before the electrochemical test. Then, 80 wt % active materials, 10 wt % single-wall carbon nanotubes (SWNTs) and 10 wt % polyvinylidene fluorides (PVDF) were mixed into N-methyl-2-pyrrolidinone (NMP). The obtained slurry was cast onto a copper foil and dried in vacuum at 50 °C for 12 h to remove the solvent. Electrochemical measurements were carried out on the CR2032 (3 V) coin-type cells with lithium metal as the counter/reference electrode, Celgard 2400 membrane as the separator, and electrolyte solution obtained by dissolving 1 M $LiPF_6$ into a mixture of ethylene carbonate (EC) and dimethyl carbonate (DMC) (EC/DMC, 1: 1, v/v). The coin cells were assembled in an Ar-filled glovebox with concentrations of moisture and oxygen below 1.0 ppm. The charge/discharge tests were performed with a NEWARE battery tester at a voltage window of 0.005–3.0 V for Co_xP samples. Cyclic voltammetry (0.005–3 V, 0.5 mV s^{-1}) was performed with an electrochemical workstation (CHI 660C).

RESULTS AND DISCUSSION

Figure 1a shows the TEM image of the sample obtained after 1 h reaction. It was observed that the products were nanorods with diameter of 10 nm and length of 50 nm (the SEM image and size distribution is shown in Supporting Information, Figure S5). The XRD result (Figure 2) showed that the peaks could be indexed to pure orthorhombic Co_2P (JCPDF NO.89–3030) with no indication of other crystal phases (The Al peaks observed in the spectra are from the substrate in the sample holder). The clear lattice fringes revealed by high-resolution TEM (HRTEM) image (Figure 1d and its inset) from a single nanorod indicated that it was single crystalline and the lattice

dx.doi.org/10.1021/am302877q | ACS Appl. Mater. Interfaces 2013, 5, 1093–1099

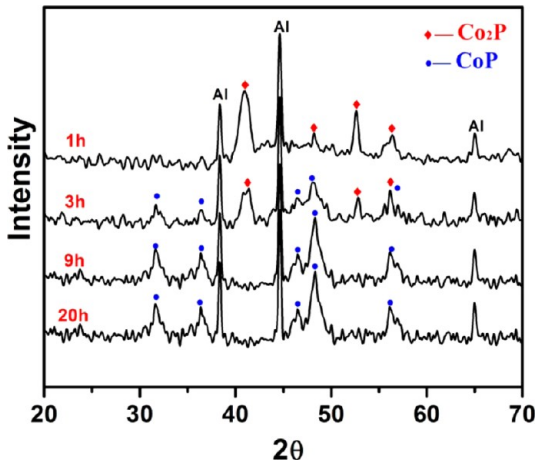

Figure 2. XRD for the products obtained at different reaction times.

distance of 0.22 nm corresponded to the (210) planes of orthorhombic Co_2P. In addition, an amorphous coating layer with a thickness of ~5 nm was observed, which was associated with the organic surfactants introduced during the reaction process.

To investigate the growth detail of the Co_xP nanocrystals, the composition and shape evolution of Co_xP samples were studied by examining intermediate products with varied reaction time from 1 to 20 h and keeping other reaction parameters unchanged (Figure 1). When the reaction time was increased to 3 h, some nanorods (as aforementioned Co_2P nanorods, see Figure 1a) were disintegrated to oval nanoparticles with a diameter of around 10 nm (see the Supporting Information, Figure S1). XRD pattern showed that the phase converted to a mixture of Co_2P and CoP (Figure 2). Here, the disintegration of Co_2P nanorods was related to the structure transformation of the Co-rich into P-rich product.[33] Interestingly, with the reaction time further extended to 9 h, the sample was found to consist of near-spherical particles with an average size of 15.6

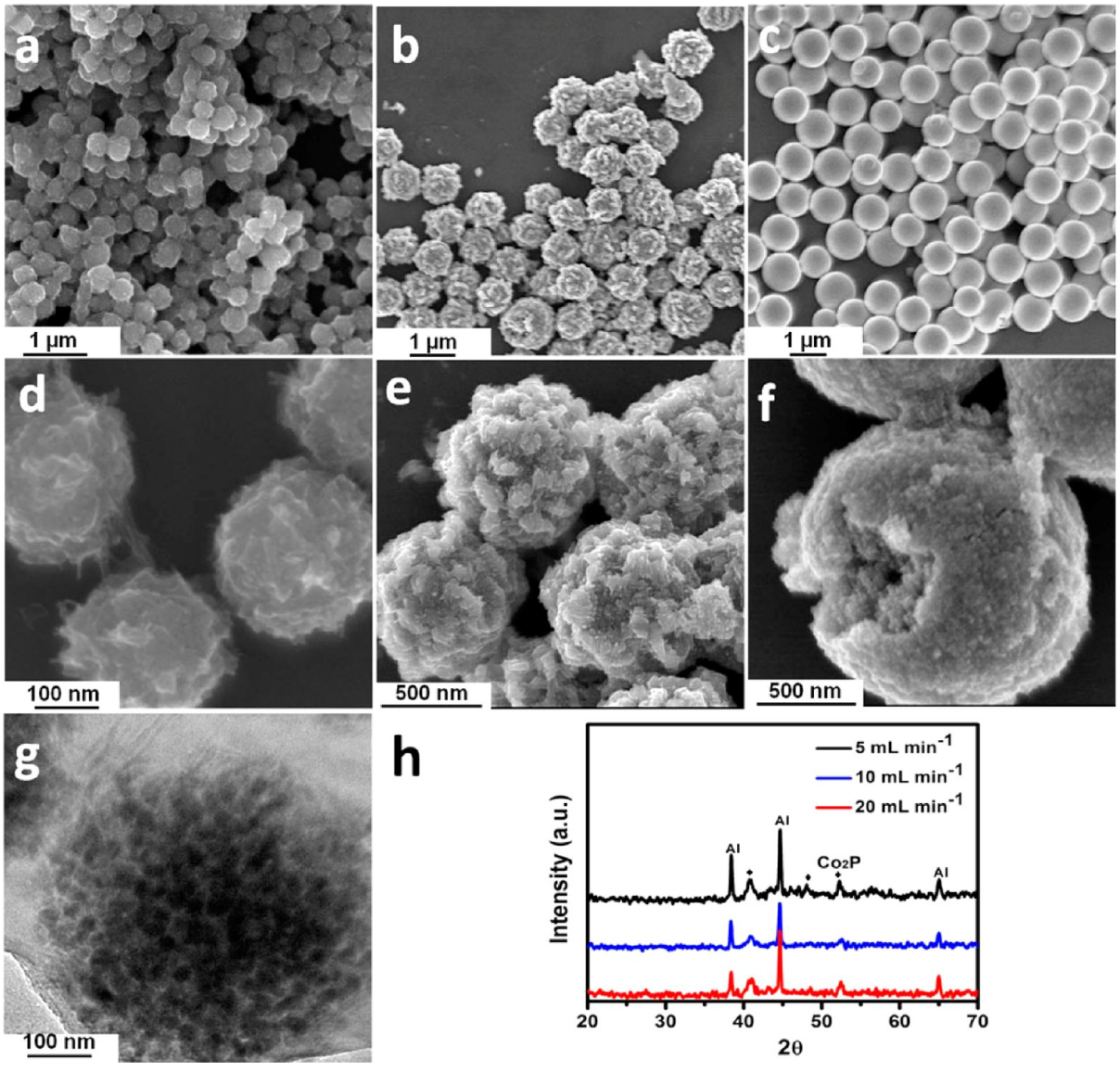

Figure 3. (a–f) FESEM images of the Co_2P spheres obtained from different injecting speed. (a) 5, (b) 10, and (c) 20 mL min^{-1}; (d–f) corresponding magnified FESEM image of a–c. (g) TEM image of sample obtained at 5 mL min^{-1}, and the other two samples are quite similar; (h) XRD pattern for Co_2P spheres obtained from different injection rate.

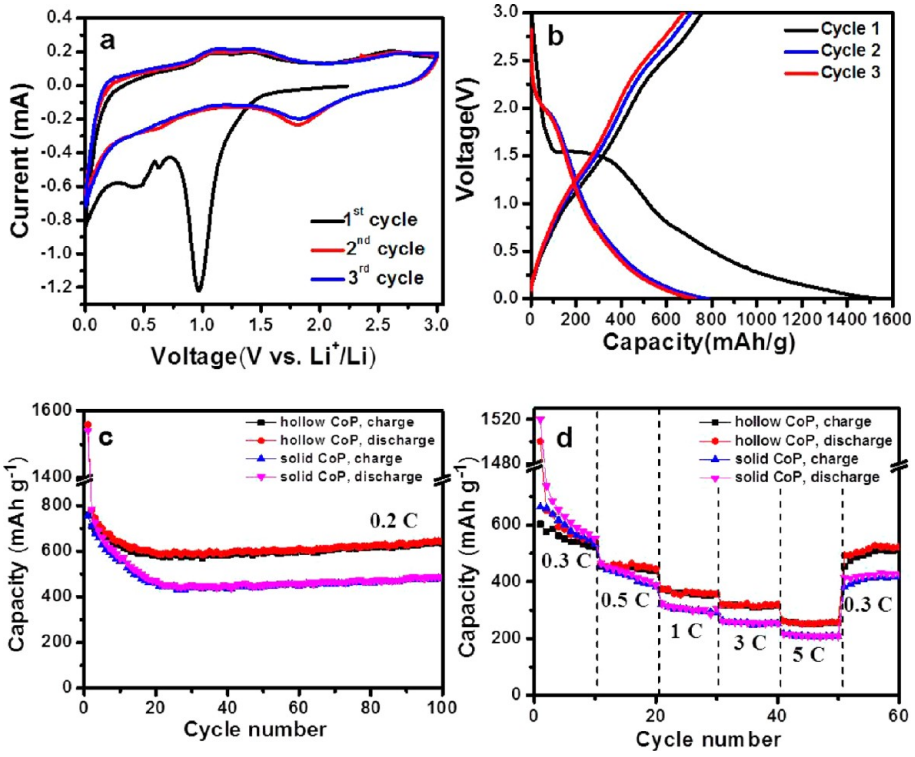

Figure 4. (a) Cyclic voltammograms (CVs) of the first three cycles of typical CoP hollow particles obtained between 0.005 and 3.0 V at a scan rate of 0.5 mv s^{-1}. (b) The charge/discharge voltage profiles of hollow CoP nanoparticles between 0.005 and 3 V (vs Li^+/Li) at a current density of 0.2 *C*; (c) cycling performance of CoP hollow and solid nanoparticles between 0.005 and 3 V (vs Li^+/Li) at 0.2 *C*; (d) comparison of charge and discharge capacities of the two electrodes at various current rates.

nm (Figure 1b and Figure S6 in the Supporting Information for size distribution). Most of these particles were hollow structures with the wall thickness of ~5 nm. XRD result showed that these hollow particles were pure orthorhombic CoP (JCPDF No. 65−1474) without any detectable impurity phases (Figure 2). It appeared that the hollow CoP particles evolved from solid particles (see the Supporting Information, Figure S1) through the nanoscale Kirkendall effect, in which the diffusion of Co in the core crossing the preformed CoP layer was faster than that of P atoms formed by the decomposition of TOP near the interface at enough high temperature.[34−36] The regular lattice fringe displayed in HRTEM image (Figure 1e) indicated that these hollow particles were single crystalline and the observed inter lattice spacings of 0.25 and 0.20 nm correspond to the (111) and (112) planes of CoP, respectively. It also showed in HRTEM that these hollow nanoparticles were encapsulated into an amorphous layer (thickness of around 1−2 nm) similar as that observed for the Co_2P nanorods. To convert this coating layer into carbon, these CoP nanoparticles were annealed at 450 °C under Ar for 2 h. The structure and the amorphous layer of CoP hollow particles retained after annealing (see the Supporting Information, Figure S2). To verify the nature of this amorphous layer, Raman characterization was carried out (see the Supporting Information, Figure S4). The signatures of G band (e.g., ~1580 cm^{-1}) and a D1 band (e.g., ~1340 cm^{-1}) indicated the existence of carbon, which was poorly crystallized and was similar as that reported for carbon formed by carbonization of organic surfactants.[37,38] Interestingly, when the reaction time was further increased to 20 h, the hollow particles disappeared and smaller nanoparticles with diameter of ~4 nm formed (see Figure S8 in the Supporting Information). These fine nanoparticles were embedded in an amorphous framework (Figure 1c, the red circles indicate grains of nanoparticle). The XRD pattern (Figure 2) was still indexed to orthorhombic CoP phase (JCPDF No. 65−1474). HRTEM image (Figure 1e) showed that they are single crystalline, and the lattice spacing between the adjacent planes is 0.25 nm, corresponding to the (111) planes of CoP. The overall description of the shape and phase evolution at different reaction times is illustrated in Figure 1g.

Except for the reaction time, the injection rate in the thermal-decomposition method also played a critical role in affecting the nucleation and growth process of nanocrystal and would finally lead to different composition and morphologies.[17,32,39,40] As mentioned before, uniform Co_2P nanorods formed when the Co-TOP complex was added dropwisely (the injection rate was 1 mL/min) into the hot oleylamine solution (Figure 1a). When slightly increasing the injection rate to 5 mL min^{-1}, we found that spheres with diameter around 200 nm were generated (Figure 3a). From the high-magnification SEM and TEM images, it was observed that these Co_2P spheres were mainly composed of ~25 nm nanoparticles (Figure 3d, g). The diameter of as-formed spheres increased to around 500 nm (Figure 3b, e) and 1 μm (Figure 3c, f) when the injecting speed was accelerated to 10 and 20 mL min^{-1}, respectively. The XRD patterns (Figure 3h) revealed that these spheres obtained at different injection rates with reaction time of 1 h were Co_2P (JCPDF NO.89−3030). A formation mechanism for these spheres was proposed.[41,42] When the Co-TOP complex was injected very fast, large amount of nuclei formed in the solution, reaching the critical point of nucleation promptly. Some of the nucleated particles needed to aggregate further in order to reduce the oversaturated nuclei concentration in a short time.

Besides, as most of TOP was consumed during the nucleation process, their capping effect to direct growth of one-dimensional (1D) structure may become less significant in the later growth process. Instead, weakly adsorbed oleylamine played a dominant role and smooth spheres composed of uniform nanoparticles were formed.

For electrochemical characterization, we first investigated the Li storage property of CoP hollow nanoparticles. For comparison purpose, solid CoP nanoparticles, prepared by tuning the volume ratio of TOP to oleylamine (see the Supporting Information, Figure S3 and S7, for detailed procedure and characterization results), were also examined. The electrochemical characterization of the samples was conducted based on a Swagelok-type cell with Li metal as the counter electrode.[43] For electrode preparation, both CoP samples were annealed at 450 °C for 2 h under Ar atmosphere to get similar carbon coated nanostructures shown in the Supporting Information Figure S3c.

A representative cyclic voltammograms (CV) of the hollow CoP nanoparticle electrodes were obtained (Figure 4a) at a scan rate of 0.5 mV s^{-1} between 0.005−3.0 V (vs Li^+/Li) for the first three discharge/charge cycles. During the first cycle discharge, a sharp peak at around 1.0 V is related to the conversion reaction: $CoP + 3\ Li^+ + 3\ e^- \rightarrow Co + Li_3P$.[44] In addition, a small peak at 0.6 V is observed, which corresponds to the reaction of $CoP + Li^+ + e^- \rightarrow LiP + Co$.[44] The broad peak appeared at 0.5 V is attributed to some irreversible reaction including the formation of solid electrolyte interphase (SEI) layer,[45,46] which is missing in subsequent charge/discharge cycles. The oxidation peaks, located at about 2.7 and 1.5 V, can be attributed to the decomposition of SEI layer and Li_3P ($Li_3P \rightarrow LiP + 2\ Li^+ + 2e^-$), respectively. The electrochemical process extended to further cycles can be characterized as a redox reaction between Li_3P and LiP: $Li_3P \leftrightarrow LiP + 2\ Li^+ + 2e^-$.[47] The second and third cycles manifest identical behavior with position and area of cathodic and anodic peaks remaining almost unchanged, indicating good reversibility and high Coulombic efficiency. The charge−discharge voltage profiles of the first three cycles were examined (Figure 4b) between 0.005 and 3 V at a current density of 89 mA g^{-1} (0.2 *C*, and 1 *C* equals to 890 mA g^{-1}). The first discharge capacity for hollow CoP particles was 1556 mA h g^{-1} and the corresponding charge capacity was 759 mA h g^{-1}. Compared to the theoretical capacity of CoP (894 mA h g^{-1}), these extra capacities were mainly resulted from the formation of a SEI layer during the first discharging process, as reported in the literatures.[39,46] This irreversible capacity loss has been widely reported for the metal phosphide electrodes, which is associated with the formation of an SEI layer.[19,48,49] During the second cycle, the CoP hollow particle electrode delivered a discharge capacity of 780 mA h g^{-1} and a charge capacity of 707 mA h g^{-1}, corresponding to a high Coulombic efficiency of 90.6%.

Stable cyclic performance of electrode is also important for practical application of LIB. Figure 4c shows the charge/discharge cycling response of CoP hollow particles at a charge/discharge rate of 0.2 *C*. The hollow CoP particles depict a discharge capacity of 630 mA h g^{-1} during the 100th cycle, which is 83.3% of the second-cycle discharge capacity. For the solid CoP electrode, a discharge capacity of only 480 mA h g^{-1} was delivered during the 100th cycle. The cycling performance of CoP electrodes at different charge/discharge rates is evaluated (Figure 4d). With increased C rates, the discharge capacity for all samples decreased gradually, indicating the diffusion-controlled kinetic process. More specifically, the CoP hollow electrode depicts ninth-cycle discharge capacities of 525, 440, 352, 314, 256 mA h g^{-1} at 0.3, 0.5, 1, 3, and 5 *C*, respectively. After the charge/discharge rate was reduced to 0.3 C, the discharge capacity could recover back to 510 mA h g^{-1}. For CoP solid particle elctrode, it depicts ninth-cycle discharge capacities of only 549, 396, 294, 252, and 208 mA h g^{-1} at 0.3, 0.5, 1, 3, and 5 *C*, respectively, which is much lower than that of hollow particles.

We also compared the Li storage properties of annealed Co_2P nanorods (shown in Figure 1a) and nanospheres composed of small nanoparticles (shown in Figure 3a). The cyclic voltammogram (CV) of Co_2P nanorods is plotted (see the Supporting Information, Figure S9). During the first cycle discharge, the reduction peak locates at 1.1 V, which corresponds to the reaction of $Co_2P + 3\ Li^+ + 3\ e^- \rightarrow 2\ Co + Li_3P$.[44] The broad peak at 0.5 V is attributed to some irreversible reaction including the formation of solid electrolyte interphase (SEI) layer.[45,46] The oxidation peaks located at around 2.7 and 1.5 V, which are attributed to the decomposition of SEI and Li_3P ($Li_3P \rightarrow LiP + 2\ Li^+ + 2e^-$), respectively. The charge−discharge voltage profiles of the first three cycles for Co_2P nanorods and spheres (see Figures S10 and S11 in the Supporting Information) tested between 0.005 and 3 V at a current density of 54 mA g^{-1} (0.2 C, and 1 C equals to 540 mA g^{-1}) showed quite similar behavior. For Co_2P nanorods, the first discharge capacity was 1300 mA h g^{-1} and the corresponding charge capacity was 600 mA h g^{-1}. During the second cycle, the electrode delivered a discharge capacity of 660 mA h g^{-1} and a charge capacity of 591 mAh g^{-1}, corresponding to a high Coulombic efficiency of 89.5%. The charge/discharge cycling performance of Co_2P electrodes was also evaluated (see the Supporting Information, Figure S12). The Co_2P nanorods depict a discharge capacity of 527 mA h g^{-1} during the 100th-cycle, which is 89.1% of the second-cycle discharge capacity. For the Co_2P spheres, a discharge capacity of only 323 mA h g^{-1} is delivered during the 100th cycle. When cycling the Co_2P electrodes at different charge/discharge rates (see the Supporting Information, Figure S13), the Co_2P nanorods depict ninth-cycle discharge capacities of 490, 385, 300, 250, and 204 mA h g^{-1} at 0.3, 0.5, 1, 3, and 5 *C*, respectively. After the charge/discharge rate was reduced to 0.3 *C*, the discharge capacity could recover back to 410 mA h g^{-1}. The Co_2P spheres depict ninth-cycle discharge capacities of only 320, 270, 200, 198, 140 mA h g^{-1} at 0.3, 0.5, 1, 3, 5 *C*, respectively, which are lower than that of nanorods.

Samples fabricated in this work showed considerable Li storage property, especially for the CoP hollow particles, which showed better performance than that of Co_xP electrodes reported in literatures.[44,45] For example, for the CoP prepared by ball milling process,[44] the capacity retained after the initial cycle was around 500 mA h g^{-1}, but this value rapidly dropped to around 350 mA h g^{-1} within the first 10 cycles. More significantly, when the Co−P electrode cycled at large current density (e.g., 1000 mA g^{-1}, around 3 C), only a capacity of 240 mA h g^{-1} can be achieved in literature,[50] lower than the 310 mA h g^{-1} obtained from hollow CoP.

Such considerable optimization in Li storage performance mainly comes from two aspects. First, as we mentioned before, the carbon shell or network obtained after annealing process can largely increase the electrical conductivity and effectively buffer the volume change, leading to highly stable cycling

performance. Second, the control over the microstructure, that is, the morphology control of the nanosized electrodes, is very crucial too. The hollow structure of CoP allows effective Li^+ insertion/extraction and accommodates the volume swing during the charge−discharge process and thus leads to enhanced specific capacities and stabilities than that of CoP solid nanoparticles. The unique one-dimensional (1D) structure of Co_2P nanorod, which can facilitate better lithium ion and electron transportation, demonstrated obvious advantage than that of the electrodes consisting of small nanoparticles in which the lithium ions and electrons have to move through these particles and are limited by the interparticle contacts.

CONCLUSION

In summary, different nanostructures of cobalt phosphides have been synthesized via a simple thermal-decomposition method and the effects of reaction time and injection rate on the composition and shape of cobalt phosphides are studied. An amorphous carbon coating layer can be generated by the carbonization of the organic surfactants on the nanostructure. Electrochemical performance of representative samples (e.g., CoP hollow and solid nanoparticles, Co_2P nanorods and spheres composed of small nanoparticles) have been investigated and showed high specific capacities, stable cyclabilities and good rate capabilities. The success in optimizing performance of cobalt phosphide electrode demonstrates that high electrochemical performance of electrode materials can be achieved with rational design of nanostructures.

ASSOCIATED CONTENT

Supporting Information

Supplementary Raman spectrum; SEM, TEM, and HRTEM images; and electrochemical performance figures. This material is available free of charge via the Internet at http://pubs.acs.org.

AUTHOR INFORMATION

Corresponding Author

*E-mail: alexyan@ntu.edu.sg.

Notes

The authors declare no competing financial interest.

ACKNOWLEDGMENTS

The authors gratefully acknowledge A*STAR SERC grant 1021700144, Singapore MPA 23/04.15.03 grant, and Singapore National Research Foundation under CREATE program: EMobility in Megacities.

REFERENCES

(1) Cabana, J.; Monconduit, L.; Larcher, D.; Palacín, M. R. *Adv. Mater.* **2010**, *22*, E170.
(2) Palacín, M. R. *Chem. Soc. Rev.* **2009**, *38*, 2565.
(3) Malini, R.; Uma, U.; Sheela, T.; Ganesan, M.; Renganathan, N. *Ionics* **2009**, *15*, 301.
(4) Lou, X. W.; Deng, D.; Lee, J. Y.; Feng, J.; Archer, L. A. *Adv. Mater.* **2008**, *20*, 258.
(5) Wu, C.; Yin, P.; Zhu, X.; OuYang, C.; Xie, Y. *J. Phy. Chem. B* **2006**, *110*, 17806.
(6) Han, S.; Jang, B.; Kim, T.; Oh, S. M.; Hyeon, T. *Adv. Funct. Mater.* **2005**, *15*, 1845.
(7) Arico, A. S.; Bruce, P.; Scrosati, B.; Tarascon, J.-M.; van Schalkwijk, W. *Nat. Mater.* **2005**, *4*, 366.
(8) Lee, K. T.; Cho, J. *Nano Today* **2011**, *6*, 28.
(9) Ji, L.; Lin, Z.; Alcoutlabi, M.; Zhang, X. *Energy Environ. Sci.* **2011**, *4*, 2682.
(10) Bruce, P. G.; Scrosati, B.; Tarascon, J.-M. *Angew. Chem., Int. Ed.* **2008**, *47*, 2930.
(11) Liu, R.; Duay, J.; Lee, S. B. *Chem. Commun.* **2011**, *47*, 1384.
(12) Hu, Y.-S.; Demir-Cakan, R.; Titirici, M.-M.; Müller, J.-O.; Schlögl, R.; Antonietti, M.; Maier, J. *Angew. Chem., Int. Ed.* **2008**, *47*, 1645.
(13) Lee, K. T.; Jung, Y. S.; Oh, S. M. *J. Am. Chem. Soc.* **2003**, *125*, 5652.
(14) Fan, J.; Wang, T.; Yu, C.; Tu, B.; Jiang, Z.; Zhao, D. *Adv. Mater.* **2004**, *16*, 1432.
(15) Zhang, Z. S.; Yang, J.; Nuli, Y.; Wang, B. F.; Xu, J. Q. *Solid State Ionics* **2005**, *176*, 693.
(16) Yang, Z. H.; Liu, L.; Wang, X. Y.; Yang, S. Y.; Su, X. P. *J. Alloys Compd.* **2011**, *509*, 165.
(17) Park, J.; Koo, B.; Yoon, K. Y.; Hwang, Y.; Kang, M.; Park, J. G.; Hyeon, T. *J. Am. Chem. Soc.* **2005**, *127*, 8433.
(18) Zhang, H. T.; Ha, D. H.; Hovden, R.; Kourkoutis, L. F.; Robinson, R. D. *Nano Lett.* **2011**, *11*, 188.
(19) Carenco, S.; Surcin, C.; Morcrette, M.; Larcher, D.; Mézailles, N.; Boissière, C.; Sanchez, C. *Chem. Mater.* **2012**, *24*, 688.
(20) Wang, H.; Shu, Y. Y.; Wang, A. Q.; Wang, J. H.; Zheng, M. Y.; Wang, X. D.; Zhang, T. *Carbon* **2008**, *46*, 2076.
(21) Brock, S. L.; Perera, S. C.; Stamm, K. L. *Chem.— Eur. J.* **2004**, *10*, 3364.
(22) Hou, H. W.; Peng, Q.; Zhang, S. Y.; Guo, Q. X.; Xie, Y. *Eur. J. Inorg. Chem.* **2005**, 2625.
(23) Ni, Y. H.; Li, J.; Jin, L.; Xia, J.; Hong, J. M.; Liao, K. M. *New J. Chem.* **2009**, *33*, 2055.
(24) Panneerselvam, A.; Nguyen, C. Q.; Waters, J.; Malik, M. A.; O'Brien, P.; Raftery, J.; Helliwell, M. *Dalton Trans.* **2008**, 4499.
(25) Schweyer-Tihay, F.; Braunstein, P.; Estournes, C.; Guille, J. L.; Lebeau, B.; Paillaud, J. L.; Richard-Plouet, M.; Rose, J. *Chem. Mater.* **2003**, *15*, 57.
(26) Ha, D. H.; Moreau, L. M.; Bealing, C. R.; Zhang, H. T.; Hennig, R. G.; Robinson, R. D. *J. Mater. Chem.* **2011**, *21*, 11498.
(27) Zhang, S. Y.; Ye, E. Y.; Liu, S. H.; Lim, S. H.; Tee, S. Y.; Dong, Z. L.; Han, M. Y. *Adv. Mater.* **2012**, *24*, 4369.
(28) Koo, J. P. B.; Hwang, Y.; Bae, C.; An, K.; Park, J. G.; Park, H. M.; Hyeon, T. *Angew. Chem., Int. Ed.* **2004**, *43*, 2282.
(29) Hall, J. W.; Membreno, N.; Wu, J.; Celio, H.; Jones, R. A.; Stevenson, K. J. *J. Am. Chem. Soc.* **2012**, *134*, 5532.
(30) Kim, Y.; Hwang, H.; Yoon, C. S.; Kim, M. G.; Cho, J. *Adv. Mater.* **2007**, *19*, 92.
(31) Maneeprakorn, W.; Malik, M. A.; O'Brien, P. *J. Mater. Chem.* **2010**, *20*, 2329.
(32) Li, Y.; Malik, M. A.; O'Brien, P. *J. Am. Chem. Soc.* **2005**, *127*, 16020.
(33) Muthuswamy, E.; Kharel, P. R.; Lawes, G.; Brock, S. L. *ACS Nano* **2009**, *3*, 2383.
(34) Ni, Y.; Tao, A.; Hu, G.; Cao, X.; Wei, X.; Yang, Z. *Nanotechnology* **2006**, *17*, 5013.
(35) Zheng, X.; Yuan, S.; Tian, Z.; Yin, S.; He, J.; Liu, K.; Liu, L. *Chem. Mater.* **2009**, *21*, 4839.
(36) Wang, J.; Johnston-Peck, A. C.; Tracy, J. B. *Chem. Mater.* **2009**, *21*, 4462.
(37) Wang, J.; Yang, Q.; Zhang, Z.; Li, T.; Zhang, S. *Dalton T.* **2010**, *39*, 227.
(38) Xu, C.; Zeng, Y.; Rui, X. H.; Xiao, N.; Zhu, J. X.; Zhang, W. Y.; Chen, J.; Liu, W. L.; Tan, H. T.; Hng, H. H.; Yan, Q. Y. *Acs Nano* **2012**, *6*, 4713.
(39) Lu, Y.; Tu, J. P.; Xiong, Q. Q.; Qiao, Y. Q.; Wang, X. L.; Gu, C. D.; Mao, S. X. *Rsc Adv.* **2012**, *2*, 3430.
(40) Qian, C.; Kim, F.; Ma, L.; Tsui, F.; Yang, P.; Liu, J. *J. Am. Chem. Soc.* **2004**, *126*, 1195.
(41) Zhang, Q.; Xie, J.; Liang, J.; Lee, J. Y. *Adv. Funct. Mater.* **2009**, *19*, 1387.

(42) Park, J.; Joo, J.; Kwon, S. G.; Jang, Y.; Hyeon, T. *Angew. Chem., Int. Ed.* **2007**, *46*, 4630.
(43) Lu, Z. Y.; Zhu, J. X.; Sim, D. H.; Zhou, W. W.; Ship, W. H.; Hng, H. H.; Yan, Q. Y. *Chem. Mater.* **2011**, *23*, 5293.
(44) Zhang, Z.; Yang, J.; Nuli, Y.; Wang, B.; Xu, J. *Solid State Ionics* **2005**, *176*, 693.
(45) López, M. C.; Ortiz, G. F.; Tirado, J. L. *J. Electrochem. Soc.* **2012**, *159*, A1253.
(46) Lu, Y.; Tu, J. P.; Xiang, J. Y.; Wang, X. L.; Zhang, J.; Mai, Y. J.; Mao, S. X. *J. Phy. Chem. C* **2011**, *115*, 23760.
(47) Lucas, I.; Perez, L.; Aroca, C.; Sánchez, P.; López, E.; Sánchez, M. C. *J. Magn. Magn. Mater.* **2005**, *290−291* (Part 2), 1513.
(48) Boyanov, S.; Zitoun, D.; Menetrier, M.; Jumas, J. C.; Womes, M.; Monconduit, L. *J. Phy. Chem. C* **2009**, *113*, 21441.
(49) Pralong, V.; Souza, D. C. S.; Leung, K. T.; Nazar, L. F. *Electrochem. Commun.* **2002**, *4*, 516.
(50) Cao, Y.; Zhou, W.; Li, X.; Ai, X.; Gao, X.; Yang, H. *Electrochim. Acta* **2006**, *51*, 4285.